A Novel Strategy for Dynamic Optimization of Grade Transition Processes Based on Molecular Weight Distribution

Jinzu Weng, Zhijiang Shao, and Xi Chen
Dept. of Control Science and Engineering, State Key Laboratory of Industrial Control Technology, Zhejiang University, Hangzhou, Zhejiang 310027, P.R. China

Xueping Gu, Zhen Yao, and Lianfang Feng
Dept. of Chemical and Biological Engineering, State Key Laboratory of Chemical Engineering, Zhejiang University, Hangzhou, Zhejiang 310027, P.R. China

Lorenz T. Biegler
Dept. of Chemical Engineering, Carnegie Mellon University, Pittsburgh, PA, 15213

DOI 10.1002/aic.14445
Published online April 2, 2014 in Wiley Online Library (wileyonlinelibrary.com)

To achieve different end-use properties of polymers, an industrial plant must produce several grades of the product through the same process under different operating conditions. As molecular weight distribution (MWD) is a crucial quality index of polymers, grade transition based on MWD is of great importance. Dynamic optimization of the grade transition process using MWD is a challenging task because of its large-scale nature. After analyzing the relationships among state variables during polymerization, a novel method is proposed to conduct the optimal grade transition using dynamic optimization with a small-scale moment model, combined with a steady-state calculation of the MWD. By avoiding expensive computation in dealing with dynamic MWD optimization, this technique greatly reduces the computational complexity of the process optimization. The theoretical equivalence of this simplification is also proved. Finally, an industrial high-density polyethylene slurry process is presented to demonstrate the efficiency and accuracy of the proposed strategy. © 2014 American Institute of Chemical Engineers *AIChE J*, 60: 2498–2512, 2014
Keywords: dynamic optimization, grade transition, molecular weight distribution

Introduction

Polymers encompass very large and broad classes of compounds with various properties, and different polymer uses require different material specifications. To achieve the different specifications for polymer end-use properties, the same process must produce several grades of the product with different qualities, under different operating conditions. These conditions require a special operating strategy called grade transition. Through grade transition one polymer grade is changed to another grade during polymerization.[1] Development of a fast and economical grade transition process has been pursued by several research groups, both in academe and in industry, over the last few decades.

Grade transition requires changes from one steady state to another to product different final products. During these changes, off-specification, low-value products are produced in transient states.[2] To decrease economic losses, plant operators must implement optimal profiles of the manipulated variables. Therefore, dynamic optimization is an important means of dealing with grade transition problems.[3] Different optimization objectives can be used to determine these optimal trajectories.[4] To address this type of problem in a systematic manner, an adequate dynamic model for the polymer grade transition process must be developed and optimized.

Many research efforts have been made to determine the optimal operating conditions of polymerization processes.[1,3–9] Cervantes et al.[4] presented an optimal control policy for an industrial low-density polyethylene plant based on average molecular weight (AMW) optimization to obtain the optimal profiles of butane fed to the plant; the results minimize the time required to reach steady-state operation and achieve new products of desirable quality. Lo and Ray[9] conducted a dynamic simulation of grade transition in an industrial fluidized bed polyethylene reactor using a nickel–diimine catalyst. They further took temperature, monomer concentration, and hydrogen composition as primary manipulated variables for achieving grade transition in terms of polymer density and target melt index. These studies, however, consider the target number AMWs (Mn), weight AMWs (Mw), or polydispersity indices (PDI), rather than the molecular weight distribution (MWD) of the quality index.

MWD is a fundamental polymer property that directly influences end-use polymer characteristics. It affects processing through the polymer melting point and the flow properties of the melted polymer. It also determines many of the mechanical properties of the processed product, such as strength and impact resistance.[10] Many methods are available

Correspondence concerning this article should be addressed to X. Chen at xichen@iipc.zju.edu.cn or L. T. Biegler at lb01@andrew.cmu.edu.

for calculating MWD, including the molecular weight moment method,[11] the Monte Carlo method,[12,13] the transformed domains method,[14–17] the discrete Galerkin method,[18,19] and the parallel computation method.[20] However, few articles have focused on determining the optimal operating policies of a target MWD. This issue has been considered in the polymerization of methyl methacrylate in batch reactors.[21–24] For continuous polyethylene production, Soares[5,25] reviewed a cumulative method that integrated an approximated Flory's distribution over time and radical location in the polymer particle to recover the MWD of the cumulative polymer by calculating the convolution of instantaneous distribution based on the quasi-steady-state approximation (QSSA). Moreover, Zapata-González et al.[26] proposed a methodology where the QSSA is applied on the fast dynamic species to reduce the stiffness, and then the remaining equations are solved by computationally inexpensive explicit algorithms. Although the Flory distribution is invalid when chain transfer reactions occur in the polymer or when the dynamic evolution of free radicals with various chain lengths is simulated, it remains very practical and useful in a many polymerization situations.

Al-haj-Ali et al.[27] addressed the issue of MWD in a single reactor during gas-phase ethylene polymerization and concluded that a broad MWD could be achieved by proper control of the hydrogen to monomer ratio inside the reactor. Pontes et al.[28] presented an optimization model for determining the optimal operating policies for tailoring polyethylene with desired MWDs in a continuous ethylene polymerization process; this model used a Ziegler–Natta catalyst in a complex configuration of continuous stirred tank reactors (CSTRs) and plug flow reactors. However, many studies[21–24,29,30] that deal with target MWDs only minimize the deviation of the calculated MWDs from the specified profile but do not care about the computational efficiency. The computational time required to solve the optimization problems takes anywhere from minutes to hours because of the complexity of the model and limitations of certain solution methods.[31]

Polymerization reactor models are necessary to describe the single process to produce a number of polymer grades featured by Mn, Mw, or PDI to satisfy the different specifications of various end-use properties. However, this practice may lead to an incomplete description of the polymer and can further mislead end-users, as polymers with similar average molecular properties may have distinct microstructural distributions and physical properties.[5] Thus, the MWD is a key in establishing quality indices for polymers. Considering MWD in the quality control and process optimization of polymer products is thus essential. However, the dynamic optimization problem involving the time evolution of MWD is difficult to solve because of its large scale, nonlinearity, and strong coupling features. Dynamic MWD optimization in a polymerization process remains a challenging task. On the one hand, the accuracy of studies that consider only the target Mn, Mw, or PDI, rather than the MWD of the formed polymer may be flawed because polymers with similar molecular properties may have distinct microstructural distributions and physical properties. On the other hand, studies that consider the MWD target must address large-scale computation problems caused by dynamic calculations of real-time MWDs.

In this article, the conventional modeling methods used in the dynamic optimization of grade transition process, including the moment method, instantaneous Flory method, and cumulative Flory method, are first presented. Then, an interesting question is raised. Can we conduct grade transition using MWD as the quality index while avoiding expensive computations to address dynamic MWD optimization? A positive answer is given in this study through theoretical analysis of the relationships among state variables. A theorem and case validation are provided to show that after selected reactor state variables in the moment model are at steady state, real-time MWDs will cease to vary. Thus, MWD dynamic optimization can be conducted by solving a small-scale dynamic moment model combined with a steady-state MWD model. Eventually, the dynamic optimization of grade transition for a high-density polyethylene (HDPE) slurry process is presented using the proposed method.

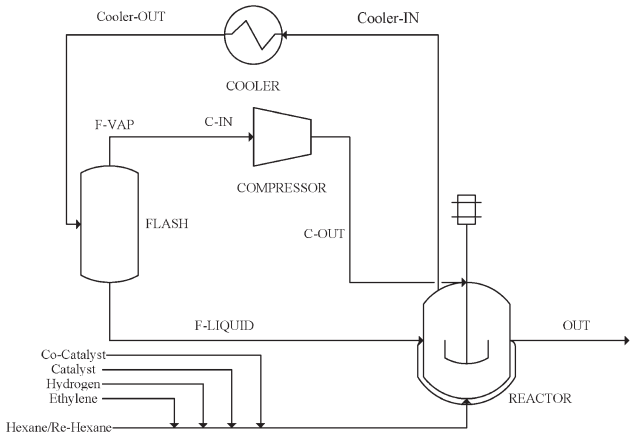

Figure 1. Flow sheet of the HDPE slurry process.

Conventional Modeling Methods

An industrial HDPE slurry process was studied in this project. Continuous slurry polymerization with multiple-site Ziegler–Natta catalysts is a typical, popular, and effective process for producing HDPE.[31] Ziegler–Natta catalyst with titanium tetrachloride [$TiCl_4$] as the primary catalyst and triethyl aluminum [$Al(C_2H_5)_3$] as the cocatalyst was used in the continuous HDPE polymerization process. Figure 1 illustrates the flow sheet of the industrial HDPE slurry process,[32] which consists of one CSTR and several other auxiliary units, including flash drums, coolers, compressors, and pumps. Ethylene (monomer), hydrogen (chain transfer agent), *n*-hexane (diluent), and the Ziegler–Natta catalyst are fed continuously into the CSTR, whereas the slurry is continuously removed from the reactor.[33] The vapor stream, Cooler-IN, which contains ethylene, hydrogen, and hexane, is recycled to the feed streams through coolers (responsible for heat removal), flash drums, and compressors to achieve high monomer conversion.

An equation-oriented model[34] was first developed for the dynamic optimization. The following assumptions were made while modeling the polymerization:

1. The gas and liquid phases in the reactor are well mixed, and phase equilibrium exists at the gas–liquid interface.
2. The mass-transfer resistance, heat transmission resistance, and diffusion at the gas–liquid interface are negligible.
3. The concentration of all the materials in the reactor is uniform.
4. The temperature of the reactor is uniform.

Table 1. Kinetic Mechanism of Homopolymerization

Reaction Types	Descriptions
Activation	$C_p(j)+A\xrightarrow{k_{aA}(j)}P_0(j)$
Initiation	$P_0(j)+M\xrightarrow{k_i(j)}P_1(j)$
Propagation	$P_n(j)+M\xrightarrow{k_p(j)}P_{n+1}(j)$
Transfer to monomer	$P_n(j)+M\xrightarrow{k_{tM}(j)}P_1(j)+D_n(j)$
Transfer to hydrogen	$P_n(j)+H_2\xrightarrow{k_{tH}(j)}P_0(j)+D_n(j)$
Transfer to cocatalyst	$P_n(j)+A\xrightarrow{k_{tA}(j)}P_0(j)+D_n(j)$
Transfer β-hydride	$P_n(j)\xrightarrow{k_t(j)}P_0(j)+D_n(j)$
Deactivation	$P_n(j)\xrightarrow{k_d(j)}C_d(j)+D_n(j)$ $P_0(j)\xrightarrow{k_d(j)}C_d(j)$

Equal reactivity is assumed, that is, the kinetic constants of propagation, transfer, and deactivation are unrelated to chain length.

The kinetic mechanism of ethylene homopolymerization with the Ziegler–Natta catalyst system is summarized in Table 1, where C_P is a potential active site of catalyst $TiCl_4$, A is the cocatalyst $Al(C_2H_5)_3$, M is the monomer, H_2 is hydrogen, P_0 is an active site, C_d is a deactivated site, D_n is a dead polymer of chain length n, P_n is the living polymer of chain length n, j is the index of the N_s active sites. Also, k_{aA} is the kinetic constant of the activation reaction, k_i is the kinetic constant of the initiation reaction, k_p is the kinetic constant of the propagation reaction, k_{tM} is the kinetic constant of the chain transfer to monomer reaction, k_{tH} is the kinetic constant of the chain transfer to hydrogen reaction, k_{tA} is the kinetic constant of the chain transfer to cocatalyst reaction, k_t is the kinetic constant of the chain transfer β-hydride reaction, and k_d is the kinetic constant of the deactivation reaction. Specifically, the chain transfer to hydrogen reaction is of order 0.5.[35]

A multisite-type catalyst model was used for this polymerization process. The number of catalyst sites (N_s) for simulating the MWD of the produced polymer was confirmed as five by deconvoluting gel permeation chromatographs (GPC) of the polymer samples.[36] The kinetic constants for these active sites were estimated using plant data from an industrial polymerization process.

The process was designed to produce multiple HDPE grades. The grade transition problem involves the dynamic computation of the product qualities of different grades and other relative states during the transition process. The conventional quality models are elaborated as follows.

Moment method

The method of moments solves the leading moments of the chain length distribution (CLD) with considerably less computational effort.[25] Then Mn, Mw, or PDI can be easily calculated from the moments of the distribution.

The mth moments of the living and dead polymers at the jth active site are, respectively

$$Y^m(j)=\sum_{n=1}^{\infty}n^m[P_n(j)] \tag{1}$$

$$X^m(j)=\sum_{n=2}^{\infty}n^m[D_n(j)] \tag{2}$$

According to the mechanism in Table 1, the following equation defines the kinetic constants for transfer and deactivation

$$K_T(j)+K_D(j)=k_{tM}(j)[M]+k_{tH}(j)[H_2]^{0.5}+k_{tA}(j)[A]+k_t(j)+k_d(j),\ \text{for}\ j=1:N_s \tag{3}$$

For the zeroth moment of the CLD of the living polymer chains, the equation can be derived by substituting the corresponding population balance into the moment expression

$$\frac{d(Y^0(j)V)}{Vdt}=k_i(j)[P_0(j)][M]-(K_T(j)+K_D(j))Y^0(j)+k_{tM}(j)[M]Y^0(j)-Y^0(j)Flowout(t)/V(t),\ \text{for}\ j=1:N_s \tag{4}$$

where *Flowout* represents the volume outflow rate, and V represents the liquid volume of the reactor.

Similarly, for the zeroth moment of CLD of the dead polymer chains, the equation takes the form

$$\frac{d(X^0(j)V)}{Vdt}=(K_T(j)+K_D(j))Y^0(j)-k_{tM}(j)[M][P_1(j)]-X^0(j)Flowout(t)/V(t),\ \text{for}\ j=1:N_s \tag{5}$$

For the first moments of CLD of the living and dead polymer chains, the equations are given by

$$\frac{d(Y^1(j)V)}{Vdt}=k_i(j)[P_0(j)][M]+k_p(j)[M]Y^0(j)-(K_T(j)+K_D(j))\times Y^1(j)+k_{tM}(j)[M]Y^0(j)-Y^1(j)Flowout(t)/V(t),\ \text{for}\ j=1:N_s \tag{6}$$

$$\frac{d(X^1(j)V)}{Vdt}=(K_T(j)+K_D(j))Y^1(j)-k_{tM}(j)[M][P_1(j)]-X^1(j)Flowout(t)/V(t),\ \text{for}\ j=1:N_s \tag{7}$$

For the second moments of CLD of the living and dead polymer chains, the equations are given by

$$\frac{d(Y^2(j)V)}{Vdt}=k_i(j)[P_0(j)][M]+k_{tM}(j)[M]Y^0(j)+k_p(j)[M](2Y^1(j)+Y^0(j))-(K_T(j)+K_D(j))Y^2(j)-Y^2(j)Flowout(t)/V(t),\ \text{for}\ j=1:N_s \tag{8}$$

$$\frac{d(X^2(j)V)}{Vdt}=(K_T(j)+K_D(j))Y^2(j)-k_{tM}(j)[M][P_1(j)]-X^2(j)Flowout(t)/V(t),\ \text{for}\ j=1:N_s \tag{9}$$

The zeroth, first, and second moments are used to calculate AMWs (the number or weight averaged MW, *Mn*, and *Mw*, respectively) as well as PDI using the following equations

$$Mn=\frac{\sum_{j=1}^{N_s}(Y^1(j)+X^1(j))}{\sum_{j=1}^{N_s}(Y^0(j)+X^0(j))}\times mw \tag{10}$$

$$Mw=\frac{\sum_{j=1}^{N_s}(Y^2(j)+X^2(j))}{\sum_{j=1}^{N_s}(Y^1(j)+X^1(j))}\times mw \tag{11}$$

$$PDI=\frac{Mw}{Mn} \tag{12}$$

where *mw* represents the molecular weight of the monomer. The moments of the living chain are much smaller

than the moments of the dead polymer; thus, the moments of the former are always ignored in the calculation of AMWs.

If the AMWs are selected as quality indexes, dynamic optimization of the grade transition can be formulated as follows

$$\begin{aligned} \min \quad & t_f \\ \text{s.t.} \quad & \dot{S}(t_f)=0 \\ & -\sigma\cdot\bar{W}_{tar} \le \bar{W}(t_f)-\bar{W}_{tar} \le \sigma\cdot\bar{W}_{tar} \\ & \dot{x}=\phi(x,u,y,t) \\ & \psi(x,u,y,t)=0 \\ & x_{lb} \le x \le x_{ub} \\ & u_{lb} \le u \le u_{ub} \\ & y_{lb} \le y \le y_{ub} \end{aligned} \tag{13}$$

where $S(t_f)$ represents the state variables at the final time t_f, including temperature, concentrations of the monomer, transfer agent, and cocatalyst, volume of reaction liquid, volume outflow rate, and moments of the living chain and dead polymer; $\dot{S}(t_f)$ is the derivative of $S(t_f)$; $\bar{W}(t_f)$ is the calculated AMW at the final time t_f; $\bar{W}_{tar}$ is the target AMW of the target grade; σ is the tolerance parameter; x is the vector of differential variables involved in the moment method; y is the vector of algebraic variables; u is the control variable; x_{lb}, u_{lb}, and y_{lb} represent the lower boundaries and x_{ub}, u_{ub}, and y_{ub} represent the upper boundaries of x, u, and y, respectively.

The objective function minimizes the transition time. The first equality constraint is included to ensure that the state variables obtain their steady-state value after t_f, indicating the end of the transition. The second inequality constraint bounds the error between the target AMWs and the calculated AMWs to ensure the quality specification for the target grade. The third and fourth equality constraints are the process models and include its thermodynamic properties, population balance, moment equations as described previously for the reactor, and a description of the behavior of the quantitative process of other unit models. The fifth, sixth, and seventh inequality constraints show the validity range of each variable.

Instantaneous Flory method

When MWD is used as the quality index, development of an MWD model is required. The conventional Flory–Schulz distribution shows the MWD of a polymer under a steady or pseudo steady-state assumption (PSSA), also called the instantaneous Flory distribution.

The weight distribution is given by[37]

$$f(j,n)=(1-\tau(j))^2(\tau(j))^{n-1}n \tag{14}$$

where n represents the chain length, and $\tau(j)$ is the distribution parameter that represents the propagation probability of the active chain at the jth active site, which can be represented as the ratio of the monomer propagation frequency over the sum of the monomer propagation frequency, chain transfer frequency, and deactivation frequency at the jth active site

$$\tau(j)=\frac{k_p(j)[M]}{k_p(j)[M]+K_T(j)+K_D(j)} \tag{15}$$

After the instantaneous Flory distributions of all of the active sites have been calculated, the instantaneous distribution of the polymer product can be obtained by averaging the distributions of each individual site type as follows[38]

$$f(n)=\sum_{j=1}^{N_s} f(j,n)mf_j \tag{16}$$

where mf_j is the weight or mass fraction of the polymer made by site type j. The parameter mf_j is defined as follows

$$mf_j=\frac{Y^1(j)+X^1(j)}{\sum_{j=1}^{N_s}(Y^1(j)+X^1(j))} \tag{17}$$

The instantaneous Flory method has a significant advantage in terms of computation speed. However, special conditions of PSSA make the application of the distribution unsuitable when the reactor is not at a steady state, for example, during grade transition. For that case, the cumulative Flory method can be introduced to calculate the time evolution of MWD.

Cumulative Flory method

During the grade transition process, the cumulative Flory distribution method can be used for the dynamic computation of MWD. Hereafter, w is used to represent the instantaneous weight, W represents cumulative weight, f represents the instantaneous distribution, and F represents the cumulative distribution.

The newly produced instantaneous total weight of the jth active site at time t is calculated as follows

$$\begin{aligned} dw(j,t)=\{&k_{tM}(j,t)[M(t)]+k_{tH}(j,t)\sqrt{[H_2(t)]}+k_{tA}(j,t)[A(t)] \\ &+k_t(j,t)+k_d(j,t)\}Y^1(j,t)V(t)dt \end{aligned} \tag{18}$$

The component for each chain length can be calculated by

$$dw(j,t,n)=dw(j,t)\ f(j,t,n)=dw(j,t)n(1-\tau(j,t))^2(\tau(j,t))^{n-1} \tag{19}$$

where n represents the chain length, $f(j,t,n)$ and $\tau(j,t)$ are the time-dependent extensions of $f(j,n)$ and $\tau(j)$ described in Eqs. 14 and 15, respectively.

For a continuous polymerization process, the inflow and outflow must also be considered. In the present case, only the outflow material needs to be considered because the feed contains no polymer. The increment of the cumulative weight for each chain length at each time interval can thus be calculated as follows

$$dW(t,n)=\sum_{j=1}^{N_s} dw(j,t,n)-W(t,n)Flowout(t)dt/V(t) \tag{20}$$

As a result, $W(t,n)$ can be calculated by dividing the whole polymerization time into a number of time intervals and applying a numerical integration method. This process is illustrated in Figure 2.

Finally, the cumulative Flory distribution can be calculated by

$$F(t,n)=\frac{W(t,n)}{\sum_{n=1}^{N_{\mathrm{MAX}}} W(t,n)} \tag{21}$$

where N_{MAX} represents the maximum chain length considered.

If the MWD is selected as the quality index, the dynamic optimization of the grade transition can be formulated as follows

$$\begin{aligned}
\min \quad & t_{\mathrm{f}} \\
\text{s.t.} \quad & \dot{S}(t_{\mathrm{f}})=0 \\
& \dot{F}(t_{\mathrm{f}},i)=0, i=1,\ldots,N_{\mathrm{p}} \\
& \sum_{i=1}^{N_{\mathrm{p}}}|F(t_{\mathrm{f}},i)-\mathrm{MWD}_{\mathrm{tar}}^{i}| \le \delta\sum_{i=1}^{N_{\mathrm{p}}}\mathrm{MWD}_{\mathrm{tar}}^{i} \\
& \dot{x}=\phi(x,u,y,t) \\
& \psi(x,u,y,t)=0 \\
& x_{\mathrm{lb}} \le x \le x_{\mathrm{ub}} \\
& u_{\mathrm{lb}} \le u \le u_{\mathrm{ub}} \\
& y_{\mathrm{lb}} \le y \le y_{\mathrm{ub}}
\end{aligned} \tag{22}$$

where MWD_{tar}^{i} is the target MWD specification; and δ is the user specified tolerance parameter. Given that consideration of the total error at each chain length between the real-time and target MWDs is impractical, a few reasonable sampling points are chosen; here, i represents the index of sampling point for chain lengths, and N_{p} is the total number of sampling points. Other symbols are identical to those described in problem (13), except that the number of differential and algebraic variables involved is greatly increased from the cumulative Flory method. Because of these large-scale features, MWD-based optimization (22) has much higher computational complexity than the moment-based optimization model in (13).

A Novel Method without Dynamic Computation of MWD

The moment method calculates the moments of living or dead polymers used for the dynamic optimization problem (13), which is relatively easy to solve. However, this may result in an incomplete description of the polymer and mislead end-users, because polymers with similar average molecular properties may have distinct microstructural distributions and physical properties. Therefore, incorporation of MWDs is essential for the quality control but the resulting dynamic optimization problem (22) is difficult to solve because of its large scale, nonlinearity, and strong coupling features. To resolve this dilemma, we now develop an efficient grade transition problem formulation that includes MWD as the quality index. Here, a combination of moment and MWD computations are used for dynamic optimization and ensure that the MWDs meet the target specification at the end of transition. Therefore, the operational result is identical to dynamic optimization (22), but only the MWD

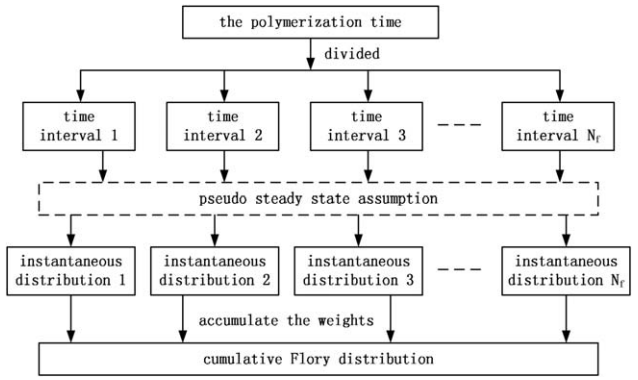

Figure 2. Process for calculating the cumulative Flory distribution.

at steady state is incorporated, that is, the instantaneous Flory distribution. Conversely, whether the cumulative MWDs also reach a steady state at the same final time is yet unknown. The following analysis sheds light on this issue.

Steady-state analysis of cumulative MWD

It is well known that steady state of the cumulative MWD implies steady state of moments and AMWs. However, the converse proposition may not be accepted. In the moment model, AMWs are output variables and state variables include temperature, concentrations of the monomer, transfer agent, and cocatalyst, volume of reaction liquid, volume outflow rate, and the moments of the living and dead polymer. If the order of the moment is expanded to the infinity, we all know that it is equivalent to the MWD model. Regarding the steady states of the two models, the following analysis shows that it is unnecessary to consider high order moments to synchronize the relationship between moments and MWDs. In fact, only the first moments $Y^1(j, t)$ are sufficient.

Definition 1. *During the grade transition process, we define t_{S} as the steady-state time required by the reactor state variables, including temperature, concentrations of the monomer, transfer agent, and cocatalyst, volume of reaction liquid, volume outflow rate, and the first moment of the living chain.*

Definition 2. *During the grade transition process, we define t_{MWD} as the steady-state time required by the reactor state variables, including the temperature, concentrations of monomer, transfer agent, and cocatalyst, the volume of reaction liquid, the volume outflow rate, and the cumulative MWD, W(t, n).*

Theorem 1. *Given*

$$\begin{aligned}
&\frac{dT(t)}{dt}=0,\frac{d[\mathrm{M}(t)]}{dt}=0,\frac{d[\mathrm{H_2}(t)]}{dt}=0,\frac{d[\mathrm{A}(t)]}{dt}=0, \\
&\frac{dV(t)}{dt}=0,\frac{d\mathrm{Flowout}\,(t)}{dt}=0,\frac{dY^1(j,t)}{dt}=0
\end{aligned} \tag{23}$$

for all $t \ge t_{\mathrm{S}}$, Then, the cumulative weight of each chain length satisfies

$$\frac{dW(t,n)}{dt}=0, \text{ for all } t \ge t_{\mathrm{S}} \tag{24}$$

where $n = 1, \ldots, N_{max}$.

Proof. When $t_{\mathrm{MWD}} \ge t_{\mathrm{S}}$, that is, when the MWD is at steady state, all moments are also at steady state and all state variables are positive.

According to the empirical Arrhenius formula

$$k(j)=k_0(j)\exp\left(-\frac{E_a(j)}{R}(1/T-1/T_{\text{ref}})\right) \tag{25}$$

As the catalyst flow rates are constant, the reaction rates are related to the temperature only and will not change after the temperature is at steady state. After t_S, the temperature, concentrations of the monomer, transfer agent, and cocatalyst, volume of reaction liquid, volume outflow rate, and first moment of the living chain are at steady state according to Definition 1. Thereafter, according to Eq. 15, the distribution parameter under the dynamic process, which can be reformulated as

$$\tau(j,t)=\frac{k_p(j,t)[\mathrm{M}(t)]}{\left(\begin{array}{c}k_p(j,t)[\mathrm{M}(t)]+k_{tM}(j,t)[\mathrm{M}(t)]+k_{tH}(j,t)\sqrt{[\mathrm{H_2}(t)]}+\\ k_{tA}(j,t)[\mathrm{A}(t)]+k_t(j,t)+k_d(j,t)\end{array}\right)} \tag{26}$$

will no longer change with time. Thus, the instantaneous weights (18) and Flory distributions (14) will not change as well. Using Eqs. 18–20, the formula for calculating the cumulative weights of each chain length can be reformulated as

$$\begin{aligned}\frac{dW(t,n)}{dt}=&\sum_{j=1}^{N_s}\{k_{tM}(j,t)[\mathrm{M}(t)]+k_{tH}(j,t)\sqrt{[\mathrm{H_2}(t)]}\\&+k_{tA}(j,t)[\mathrm{A}(t)]+k_t(j,t)+k_d(j,t)\}Y^1(j,t)V(t)\\&\times n(1-\tau(j,t))^2(\tau(j,t))^{n-1}\\&-W(t,n)Flowout(t)/V(t)\end{aligned} \tag{27}$$

Defining

$$C_0(t)=Flowout(t)/V(t) \tag{28}$$

leads to

$$\begin{aligned}C_{1,n}(t)=&\sum_{j=1}^{N_s}\{k_{tM}(j,t)[\mathrm{M}(t)]+k_{tH}(j,t)\sqrt{[\mathrm{H_2}(t)]}\\&+k_{tA}(j,t)[\mathrm{A}(t)]+k_t(j,t)+k_d(j,t)\}Y^1(j,t)V(t)\\&\times n(1-\tau(j,t))^2(\tau(j,t))^{n-1}\end{aligned} \tag{29}$$

and (27) can be written as

$$\frac{dW(t,n)}{dt}=C_{1,n}(t)-C_0(t)W(t,n) \tag{30}$$

where we consider the initial condition given at t_S. According to Definition 1, when $t \geq t_S$, $C_0(t)$, and $C_{1,n}(t)$ are constant. Hence, substituting the constants C_0 and $C_{1,n}$ into (30) leads to the following solution

$$W(t,n)=\left(W(t_S,n)-\frac{C_{1,n}}{C_0}\right)e^{-C_0(t-t_S)}+\frac{C_{1,n}}{C_0},\ t \geq t_S \tag{31}$$

According to Definition 2

$$W(t_1,n)=W(t_{\text{MWD}},n),\forall t_1 > t_{\text{MWD}} \tag{32}$$

and the fact that

$$t_{\text{MWD}} \geq t_S \tag{33}$$

we combine Eqs. 31 and 32 to yield

$$\begin{aligned}&\left(W(t_S,n)-\frac{C_{1,n}}{C_0}\right)e^{-C_0(t_1-t_S)}+\frac{C_{1,n}}{C_0}\\&=\left(W(t_S,n)-\frac{C_{1,n}}{C_0}\right)e^{-C_0(t_{\text{MWD}}-t_S)}+\frac{C_{1,n}}{C_0}\end{aligned} \tag{34}$$

$$\left(W(t_S,n)-\frac{C_{1,n}}{C_0}\right)\left(e^{-C_0t_1}-e^{-C_0t_{\text{MWD}}}\right)e^{C_0t_S}=0 \tag{35}$$

Because

$$\left(e^{-C_0t_1}-e^{-C_0t_{\text{MWD}}}\right)e^{C_0t_S} \neq 0,\forall t_1 > t_{\text{MWD}} \tag{36}$$

we have

$$W(t_S,n)-\frac{C_{1,n}}{C_0}=0 \tag{37}$$

and Eq. 31 then yields

$$W(t,n)=\left(W(t_S,n)-\frac{C_{1,n}}{C_0}\right)e^{-C_0t}+\frac{C_{1,n}}{C_0}=\frac{C_{1,n}}{C_0},\quad t \geq t_S \tag{38}$$

Finally, substituting Eq. 38 into Eq. 30 yields

$$\frac{dW(t,n)}{dt}=C_{1,n}-C_0W(t,n)=C_{1,n}-C_0\frac{C_{1,n}}{C_0}=0,\quad t \geq t_S \tag{39}$$

Q.E.D.

Remark. *Theorem 1 proves that both state variables mentioned in Definition 1 and cumulative MWD reach steady states at the same time. Thus, we can combine the moment model and steady-state MWD computation to solve the grade transition problem. In practice, however, Eq. 23 is not easy to implement and inequalities with tolerances are normally used instead. Theorem 1 can be extended to deal with these tolerances as follows.*

Theorem 2. *Given the tolerance on all state variables, $\alpha > 0$, which, during the grade transition process, applies over $t_\alpha \leq t \leq t_S$, such that*

$$T(t_S)(1-\alpha) \leq T(t) \leq T(t_S)(1+\alpha) \tag{40}$$

$$\mathrm{M}(t_S)(1-\alpha) \leq \mathrm{M}(t) \leq \mathrm{M}(t_S)(1+\alpha) \tag{41}$$

$$\mathrm{H_2}(t_S)(1-\alpha) \leq \mathrm{H_2}(t) \leq \mathrm{H_2}(t_S)(1+\alpha) \tag{42}$$

$$\mathrm{A}(t_S)(1-\alpha) \leq \mathrm{A}(t) \leq \mathrm{A}(t_S)(1+\alpha) \tag{43}$$

$$V(t_S)(1-\alpha) \leq V(t) \leq V(t_S)(1+\alpha) \tag{44}$$

$$Flowout(t_S)(1-\alpha) \leq Flowout(t) \leq Flowout(t_S)(1+\alpha) \tag{45}$$

$$Y^1(j,t_S)(1-\alpha) \leq Y^1(j,t) \leq Y^1(j,t_S)(1+\alpha) \tag{46}$$

Then for $t_\alpha \leq t \leq t_S$, a relative error $\varepsilon > 0$, which is dependent of α, exists such that

$$\begin{aligned}&-\frac{2\varepsilon}{(1-\varepsilon)}e^{C_0(t_S)(1-\varepsilon)(t_S-t_\alpha)}+\frac{2\varepsilon}{(1-\varepsilon)} \leq \frac{W(t,n)-W(t_S,n)}{W(t_S,n)}\\&\leq \frac{2\varepsilon}{(1+\varepsilon)}e^{C_0(t_S)(1+\varepsilon)(t_S-t_\alpha)}-\frac{2\varepsilon}{(1+\varepsilon)}\end{aligned} \tag{47}$$

Proof. According to Theorem 1, the following equation can be obtained

$$W(t_S,n)=\frac{C_{1,n}(t_S)}{C_0(t_S)} \tag{48}$$

For $C_0(t)$, according to Eq. 28 and the tolerance α, when $t_\alpha \leq t \leq t_S$,

$$\frac{\text{Flowout}(t_S)(1-\alpha)}{V(t_S)(1+\alpha)} \leq C_0(t) \leq \frac{\text{Flowout}(t_S)(1+\alpha)}{V(t_S)(1-\alpha)} \tag{49}$$

$$C_0(t_S)\left(1-\frac{2\alpha}{1+\alpha}\right) \leq C_0(t) \leq C_0(t_S)\left(1+\frac{2\alpha}{1-\alpha}\right) \tag{50}$$

For $C_{1,n}(t)$, according to the tolerance α and empirical Arrhenius formula

$$k(j,t)=k_0(j)\exp\left(-\frac{E_a(j)}{R}(1/T(t)-1/T_{ref})\right) \quad (51)$$

when $t_\alpha \le t \le t_S$

$$k_0(j)\exp\left(\frac{E_a(j)}{RT_{ref}}\right)\exp\left(-\frac{E_a(j)}{RT(t_S)(1-\alpha)}\right) \le k(j,t) \le k_0(j)\exp\left(\frac{E_a(j)}{RT_{ref}}\right)\exp\left(-\frac{E_a(j)}{RT(t_S)(1+\alpha)}\right) \quad (52)$$

we can define a positive constant

$$\beta=\max_j\left\{1-\exp\left(-\frac{\alpha E_a(j)}{RT(t_S)(1-\alpha)}\right),\exp\left(\frac{\alpha E_a(j)}{RT(t_S)(1+\alpha)}\right)-1\right\} \quad (53)$$

which satisfies

$$k(j,t_S)(1-\beta) \le k(j,t) \le k(j,t_S)(1+\beta) \quad (54)$$

Using Eqs. 54 and 26 and the tolerance α, when $t_\alpha \le t \le t_S$, leads to

$$\tau(j,t) \ge \frac{k_p(j,t_S)(1-\beta)[M(t_S)](1-\alpha)}{\{k_p(j,t_S)(1+\beta)[M(t_S)](1+\alpha)+k_{tM}(j,t_S)(1+\beta)[M(t_S)](1+\alpha)+ k_{tH}(j,t_S)(1+\beta)\sqrt{[H_2(t_S)](1+\alpha)}+k_{tA}(j,t_S)(1+\beta)[A(t_S)](1+\alpha)+ k_t(j,t_S)(1+\beta)+k_d(j,t_S)(1+\beta)\}} \quad (55)$$

$$\tau(j,t) \le \frac{k_p(j,t_S)(1+\beta)[M(t_S)](1+\alpha)}{\{k_p(j,t_S)(1-\beta)[M(t_S)](1-\alpha)+k_{tM}(j,t_S)(1-\beta)[M(t_S)](1-\alpha)+ k_{tH}(j,t_S)(1-\beta)\sqrt{[H_2(t_S)](1-\alpha)}+k_{tA}(j,t_S)(1-\beta)[A(t_S)](1-\alpha)+ k_t(j,t_S)(1-\beta)+k_d(j,t_S)(1-\beta)\}} \quad (56)$$

We then define a positive constant

$$\gamma=max\left\{1-\frac{(1-\alpha)(1-\beta)}{(1+\alpha)(1+\beta)},\frac{(1+\alpha)(1+\beta)}{(1-\alpha)(1-\beta)}-1\right\} \quad (57)$$

which satisfies

$$\tau(j,t_S)(1-\gamma) \le \tau(j,t) \le \tau(j,t_S)(1+\gamma) \quad (58)$$

According to Eq. 29 and the tolerance α, when $t_\alpha \le t \le t_S$

$$C_{1,n}(t) \ge \sum_{j=1}^{N_s}\{k_{tM}(j,t_S)(1-\beta)[M(t_S)](1-\alpha) + k_{tH}(j,t_S)(1-\beta)\sqrt{[H_2(t_S)](1-\alpha)}+k_{tA}(j,t_S)(1-\beta)[A(t_S)] \times(1-\alpha)+k_t(j,t_S)(1-\beta)+k_d(j,t_S)(1-\beta)\}Y^1(j,t_S)(1-\alpha) \times V(t_S)(1-\alpha)n(1-\tau(j,t_S)(1+\gamma))^2(\tau(j,t_S))^{n-1}(1-\gamma)^{n-1} \quad (59)$$

$$C_{1,n}(t) \le \sum_{j=1}^{N_s}\{k_{tM}(j,t_S)(1+\beta)[M(t_S)](1+\alpha) + k_{tH}(j,t_S)(1+\beta)\sqrt{[H_2(t_S)](1+\alpha)}+k_{tA}(j,t_S) \times(1+\beta)[A(t_S)](1+\alpha)+k_t(j,t_S)(1+\beta)+k_d(j,t_S)(1+\beta)\} \times Y^1(j,t_S)(1+\alpha)V(t_S)(1+\alpha)n(1-\tau(j,t_S)(1-\gamma))^2 \times(\tau(j,t_S))^{n-1}(1+\gamma)^{n-1} \quad (60)$$

Finally, we can define a positive constant

$$\lambda=\max_j\{1-min\{(1-\beta)(1-\alpha)^3(1-\gamma)^{n-1} \times\left(\frac{1-(1+\gamma)\tau(j,t_S)}{1-\tau(j,t_S)}\right)^2\},max\{(1+\beta)(1+\alpha)^3(1+\gamma)^{n-1} \times\left(\frac{1-(1-\gamma)\tau(j,t_S)}{1-\tau(j,t_S)}\right)^2\}-1\} \quad (61)$$

which satisfies

$$C_{1,n}(t_S)(1-\lambda) \le C_{1,n}(t) \le C_{1,n}(t_S)(1+\lambda) \quad (62)$$

Thus, a relative error $\varepsilon=\max\left\{\frac{2\alpha}{1-\alpha},\lambda\right\}$ exists, which satisfies

$$C_0(t_S)(1-\varepsilon) \le C_0(t) \le C_0(t_S)(1+\varepsilon) \quad (63)$$

$$C_{1,n}(t_S)(1-\varepsilon) \le C_{1,n}(t) \le C_{1,n}(t_S)(1+\varepsilon) \quad (64)$$

According to Eq. 30 and the inequalities in (63) and (64) when $t_\alpha \le t \le t_S$

$$C_{1,n}(t_S)(1-\varepsilon)-C_0(t_S)(1+\varepsilon)W(t,n) \le \frac{dW(t,n)}{dt}=C_{1,n}(t)-C_0(t)W(t,n) \quad (65)$$

$$\frac{dW(t,n)}{dt}=C_{1,n}(t)-C_0(t)W(t,n) \le C_{1,n}(t_S)(1+\varepsilon)-C_0(t_S)(1-\varepsilon)W(t,n) \quad (66)$$

For the inequality (65), there exists $P(t) \ge 0, t_\alpha \le t \le t_S$, which satisfies

$$P(t)+C_{1,n}(t_S)(1-\varepsilon)-C_0(t_S)(1+\varepsilon)W(t,n)=\frac{dW(t,n)}{dt} \quad (67)$$

The general solution of Eq. 67 is as follows

$$W(t,n)=Ce^{C_0(t_S)(1+\varepsilon)(t_S-t)}+ e^{C_0(t_S)(1+\varepsilon)(t_S-t)}\int_{t_S}^{t}(P(t')+C_{1,n}(t_S)(1-\varepsilon))e^{C_0(t_S)(1+\varepsilon)(t'-t_S)}dt' \quad (68)$$

where C represents an constant and $t_\alpha \le t \le t_S$
At time t_S

$$W(t_S,n)=Ce^{C_0(t_S)(1+\varepsilon)(t_S-t_S)}+ e^{C_0(t_S)(1+\varepsilon)(t_S-t_S)}\int_{t_S}^{t_S}(P(t)+C_{1,n}(t_S)(1-\varepsilon))e^{C_0(t_S)(1+\varepsilon)(t-t_S)}dt =C \quad (69)$$

Substituting Eq. 69 into Eq. 68 yields the following solution

$$W(t,n)=W(t_S,n)e^{C_0(t_S)(1+\varepsilon)(t_S-t)}+$$
$$e^{C_0(t_S)(1+\varepsilon)(t_S-t)}\int_{t_S}^{t}(P(t')+C_{1,n}(t_S)(1-\varepsilon))e^{C_0(t_S)(1+\varepsilon)(t'-t_S)}dt' \tag{70}$$

Given that

$$\begin{gathered}e^{C_0(t_S)(1+\varepsilon)(t_S-t)}>0\\ e^{C_0(t_S)(1+\varepsilon)(t-t_S)}>0\\ P(t)\geq 0\end{gathered} \tag{71}$$

we have for $t<t_S$

$$\begin{aligned}&W(t,n)=W(t_S,n)e^{C_0(t_S)(1+\varepsilon)(t_S-t)}+\\ &e^{C_0(t_S)(1+\varepsilon)(t_S-t)}\int_{t_S}^{t}(P(t')+C_{1,n}(t_S)(1-\varepsilon))e^{C_0(t_S)(1+\varepsilon)(t'-t_S)}dt'\\ &\leq W(t_S,n)e^{C_0(t_S)(1+\varepsilon)(t_S-t)}+\\ &e^{C_0(t_S)(1+\varepsilon)(t_S-t)}\int_{t_S}^{t}C_{1,n}(t_S)(1-\varepsilon)e^{C_0(t_S)(1+\varepsilon)(t'-t_S)}dt'\end{aligned} \tag{72}$$

where $C_{1,n}(t_S)(1-\varepsilon)$ is a constant independent of time. Thus

$$\begin{aligned}W(t,n)&\leq W(t_S,n)e^{C_0(t_S)(1+\varepsilon)(t_S-t)}+C_{1,n}(t_S)(1-\varepsilon)e^{C_0(t_S)(1+\varepsilon)(t_S-t)}\int_{t_S}^{t}e^{C_0(t_S)(1+\varepsilon)(t'-t_S)}dt'\\ &=W(t_S,n)e^{C_0(t_S)(1+\varepsilon)(t_S-t)}+\frac{C_{1,n}(t_S)(1-\varepsilon)}{C_0(t_S)(1+\varepsilon)}e^{C_0(t_S)(1+\varepsilon)(t_S-t)}(e^{C_0(t_S)(1+\varepsilon)(t-t_S)}-1)\\ &=W(t_S,n)e^{C_0(t_S)(1+\varepsilon)(t_S-t)}+\frac{C_{1,n}(t_S)(1-\varepsilon)}{C_0(t_S)(1+\varepsilon)}-\frac{C_{1,n}(t_S)(1-\varepsilon)}{C_0(t_S)(1+\varepsilon)}e^{C_0(t_S)(1+\varepsilon)(t_S-t)}\end{aligned} \tag{73}$$

Substituting Eq. 48 into Eq. 73 gives

$$\begin{aligned}W(t,n)&\leq\left(\frac{C_{1,n}(t_S)}{C_0(t_S)}-\frac{C_{1,n}(t_S)(1-\varepsilon)}{C_0(t_S)(1+\varepsilon)}\right)e^{C_0(t_S)(1+\varepsilon)(t_S-t)}\\ &+\frac{C_{1,n}(t_S)(1-\varepsilon)}{C_0(t_S)(1+\varepsilon)}\\ &=\left(\frac{2\varepsilon C_{1,n}(t_S)}{C_0(t_S)(1+\varepsilon)}\right)e^{C_0(t_S)(1+\varepsilon)(t_S-t)}+\frac{C_{1,n}(t_S)(1-\varepsilon)}{C_0(t_S)(1+\varepsilon)}\\ &=\frac{2\varepsilon}{(1+\varepsilon)}W(t_S,n)e^{C_0(t_S)(1+\varepsilon)(t_S-t)}+\frac{(1-\varepsilon)}{(1+\varepsilon)}W(t_S,n)\\ &=\left(\frac{2\varepsilon}{(1+\varepsilon)}e^{C_0(t_S)(1+\varepsilon)(t_S-t)}-\frac{2\varepsilon}{(1+\varepsilon)}+1\right)W(t_S,n)\end{aligned} \tag{74}$$

and for $t_\alpha\leq t\leq t_S$

$$W(t,n)\leq\left(\frac{2\varepsilon}{(1+\varepsilon)}e^{C_0(t_S)(1+\varepsilon)(t_S-t_\alpha)}-\frac{2\varepsilon}{(1+\varepsilon)}+1\right)W(t_S,n) \tag{75}$$

which gives the upper bound for (47).

Now for the inequality (66), there exists $Q(t)\geq 0, t_\alpha\leq t\leq t_S$, which satisfies

$$\frac{dW(t,n)}{dt}=C_{1,n}(t_S)(1+\varepsilon)-C_0(t_S)(1-\varepsilon)W(t,n)-Q(t) \tag{76}$$

By analogy, the general solution of Eq. 76 is as follows

$$\begin{aligned}&W(t,n)=Ce^{C_0(t_S)(1-\varepsilon)(t_S-t)}+\\ &e^{C_0(t_S)(1-\varepsilon)(t_S-t)}\int_{t_S}^{t}\left(C_{1,n}(t_S)(1+\varepsilon)-Q(t')\right)e^{C_0(t_S)(1-\varepsilon)(t'-t_S)}dt'\end{aligned} \tag{77}$$

where C represents a constant and $t_\alpha\leq t\leq t_S$

At time t_S

$$\begin{aligned}&W(t_S,n)=Ce^{C_0(t_S)(1-\varepsilon)(t_S-t_S)}+\\ &e^{C_0(t_S)(1-\varepsilon)(t_S-t_S)}\int_{t_S}^{t_S}\left(C_{1,n}(t_S)(1+\varepsilon)-Q(t')\right)e^{C_0(t_S)(1-\varepsilon)(t'-t_S)}dt'\\ &=C\end{aligned} \tag{78}$$

Substituting Eq. 78 into Eq. 77 yields the following solution

$$\begin{aligned}&W(t,n)=W(t_S,n)e^{C_0(t_S)(1-\varepsilon)(t_S-t)}+\\ &e^{C_0(t_S)(1-\varepsilon)(t_S-t)}\int_{t_S}^{t}\left(C_{1,n}(t_S)(1+\varepsilon)-Q(t')\right)e^{C_0(t_S)(1-\varepsilon)(t'-t_S)}dt'\end{aligned} \tag{79}$$

Given that

$$\begin{gathered}e^{C_0(t_S)(1-\varepsilon)(t_S-t)}>0\\ e^{C_0(t_S)(1-\varepsilon)(t-t_S)}>0\\ Q(t)\geq 0\end{gathered} \tag{80}$$

we have

$$\begin{aligned}&W(t,n)=W(t_S,n)e^{C_0(t_S)(1-\varepsilon)(t_S-t)}+\\ &e^{C_0(t_S)(1-\varepsilon)(t_S-t)}\int_{t_S}^{t}(C_{1,n}(t_S)(1+\varepsilon)-Q(t'))e^{C_0(t_S)(1-\varepsilon)(t'-t_S)}dt'\\ &\geq W(t_S,n)e^{C_0(t_S)(1-\varepsilon)(t_S-t)}+\\ &e^{C_0(t_S)(1-\varepsilon)(t_S-t)}\int_{t_S}^{t}C_{1,n}(t_S)(1+\varepsilon)e^{C_0(t_S)(1-\varepsilon)(t'-t_S)}dt'\end{aligned} \tag{81}$$

where $C_{1,n}(t_S)(1+\varepsilon)$ is a constant independent of time. Thus

$$\begin{aligned}W(t,n)&\geq W(t_S,n)e^{C_0(t_S)(1-\varepsilon)(t_S-t)}+C_{1,n}(t_S)(1+\varepsilon)e^{C_0(t_S)(1-\varepsilon)(t_S-t)}\int_{t_S}^{t}e^{C_0(t_S)(1-\varepsilon)(t'-t_S)}dt'\\ &=W(t_S,n)e^{C_0(t_S)(1-\varepsilon)(t_S-t)}+\frac{C_{1,n}(t_S)(1+\varepsilon)}{C_0(t_S)(1-\varepsilon)}e^{C_0(t_S)(1-\varepsilon)(t_S-t)}(e^{C_0(t_S)(1-\varepsilon)(t-t_S)}-1)\\ &=W(t_S,n)e^{C_0(t_S)(1-\varepsilon)(t_S-t)}+\frac{C_{1,n}(t_S)(1+\varepsilon)}{C_0(t_S)(1-\varepsilon)}-\frac{C_{1,n}(t_S)(1+\varepsilon)}{C_0(t_S)(1-\varepsilon)}e^{C_0(t_S)(1-\varepsilon)(t_S-t)}\end{aligned} \tag{82}$$

Substituting Eq. 48 into Eq. 82 gives

$$\begin{aligned} W(t,n) &\geq \left(\frac{C_{1,n}(t_S)}{C_0(t_S)} - \frac{C_{1,n}(t_S)(1+\varepsilon)}{C_0(t_S)(1-\varepsilon)}\right) e^{C_0(t_S)(1-\varepsilon)(t_S-t)} \\ &\quad + \frac{C_{1,n}(t_S)(1+\varepsilon)}{C_0(t_S)(1-\varepsilon)} \\ &= \left(-\frac{2\varepsilon C_{1,n}(t_S)}{C_0(t_S)(1-\varepsilon)}\right) e^{C_0(t_S)(1-\varepsilon)(t_S-t)} + \frac{C_{1,n}(t_S)(1+\varepsilon)}{C_0(t_S)(1-\varepsilon)} \\ &= -\frac{2\varepsilon}{(1-\varepsilon)} W(t_S,n) e^{C_0(t_S)(1-\varepsilon)(t_S-t)} + \frac{(1+\varepsilon)}{(1-\varepsilon)} W(t_S,n) \\ &= \left(-\frac{2\varepsilon}{(1-\varepsilon)} e^{C_0(t_S)(1-\varepsilon)(t_S-t)} + \frac{2\varepsilon}{(1-\varepsilon)} + 1\right) W(t_S,n) \end{aligned} \tag{83}$$

and for $t_\alpha \leq t \leq t_S$

$$W(t,n) \geq \left(-\frac{2\varepsilon}{(1-\varepsilon)} e^{C_0(t_S)(1-\varepsilon)(t_S-t_\alpha)} + \frac{2\varepsilon}{(1-\varepsilon)} + 1\right) W(t_S,n) \tag{84}$$

Thus from Eqs. 75 and 84

$$\begin{aligned} &-\frac{2\varepsilon}{(1-\varepsilon)} e^{C_0(t_S)(1-\varepsilon)(t_S-t_\alpha)} + \frac{2\varepsilon}{(1-\varepsilon)} \leq \frac{W(t,n)-W(t_S,n)}{W(t_S,n)} \\ &\leq \frac{2\varepsilon}{(1+\varepsilon)} e^{C_0(t_S)(1+\varepsilon)(t_S-t_\alpha)} - \frac{2\varepsilon}{(1+\varepsilon)} \end{aligned} \tag{85}$$

Q.E.D.

Remark. *Theorem 2 shows that if the tolerance of the state variables, α, is small enough, the difference between $W(t,n)$ and $W(t_S,n)$ will be acceptably small as well.*

Dynamic optimization formulation based on Theorems 1 and 2

Based on Theorems 1 and 2, we can extend dynamic optimization with the moment method (13) by adding the steady-state MWD model (14)–(17). The dynamic optimization of the grade transition can thus be formulated as follows

$$\begin{aligned} \min \quad & t_f \\ \text{s.t.} \quad & \dot{S}(t_f) = 0 \\ & \sum_{i=1}^{N_p} \left| f(t_f,i) - \mathrm{MWD}^i_{tar} \right| \leq \delta \sum_{i=1}^{N_p} \mathrm{MWD}^i_{tar} \\ & \dot{x} = \phi(x,u,y,t) \\ & \psi(x,u,y,t) = 0 \\ & x_{lb} \leq x \leq x_{ub} \\ & u_{lb} \leq u \leq u_{ub} \\ & y_{lb} \leq y \leq y_{ub} \end{aligned} \tag{86}$$

where S are the state variables shown in Theorem 1; $f(t_f, i)$ is the ith sampling point of instantaneous MWD obtained at the final time, t_f; N_p is the number of sampling points; MWD^i_{tar} is the target MWD value at the ith sampling point; and δ is the tolerance parameter given by users.

This optimization problem is a variation of Problem (13) by replacing the AMW with MWD. Compared with Problem (22), which is the direct formulation for dynamic optimization with MWD, the computation complexity in Problem (86) has been greatly reduced as only steady-state MWD calculations based on the instantaneous method are required. According to Theorem 1, the first equality constraint determines whether or not the grade transition process has reached a steady state. The second constraint is required to ensure at steady state that the MWD is the target MWD; this prevents the transition to the same average molecular property but with different MWDs.

The first equality constraint in Problem (86) requires the transition to be terminated only after the process is completely at a steady state. However, satisfying this equality constraint may lead to a large and impractical transition time. Based on the theoretical analysis in Theorem 2, we modify Problem (86) using a relaxed inequality constraint to substitute for the first equality constraint as shown below

$$\begin{aligned} \min \quad & t_f \\ \text{s.t.} \quad & -\eta S(t_f) \leq S(t_f) - S(t_k) \leq \eta S(t_f) \\ & \sum_{i=1}^{N_p} \left| f(t_f,i) - \mathrm{MWD}^i_{tar} \right| \leq \delta \sum_{i=1}^{N_p} \mathrm{MWD}^i_{tar} \\ & \dot{x} = \phi(x,u,y,t) \\ & \psi(x,u,y,t) = 0 \\ & x_{lb} \leq x \leq x_{ub} \\ & u_{lb} \leq u \leq u_{ub} \\ & y_{lb} \leq y \leq y_{ub} \end{aligned} \tag{87}$$

where $S(t_f)$ is the state variable calculated at the final time t_f; $S(t_k)$ is the state variable calculated at time t_k, which is set to $0.95^* t_f$; and η and δ are both tolerance parameters. The other symbols in the equation are identical to those used in problems (13) and (22).

The relationships among the previous methods and the new method are illustrated and compared in Figure 3. The new method, as shown in the right hand of the figure, combines dynamic optimization using the moment method (13) and steady-state calculations of the MWD using the instantaneous Flory method (14)–(17). Dynamic optimization (13) ensures that the process can transition to a new steady grade, while the instantaneous Flory method guarantees that the transition grade is the target grade with specifications at the molecular level. Theorems 1 and 2 support the synchronization between moments and MWD. The advantage of the new strategy is that it enforces desired product at the target MWD while avoiding computations of the dynamic cumulative MWD during grade transition.

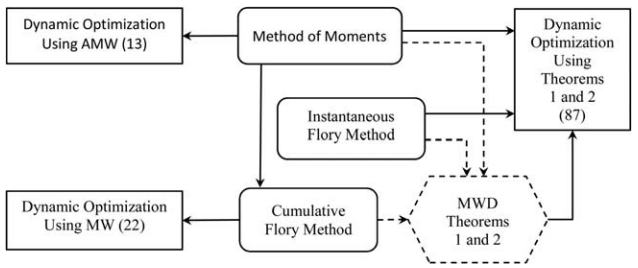

Figure 3. Relationship and implementation structure of the used methods.

Table 2. Steady-State Operating Conditions of Grades A, B, C, and D

	Grade A	Grade B	Grade C	Grade D
Catalyst feed	0.743 (kmol/h)	1.169 (kmol/h)	0.748 (kmol/h)	0.361 (kmol/h)
Cocatalyst feed	0.768 (kmol/h)	0.734 (kmol/h)	0.947 (kmol/h)	0.843 (kmol/h)
Hydrogen feed	2.108 (kmol/h)	2.3014 (kmol/h)	4.652 (kmol/h)	4.046 (kmol/h)
Monomer feed	107.633 (kmol/h)	104.806 (kmol/h)	128.402 (kmol/h)	122.663 (kmol/h)
Hexane feed	79.491 (kmol/h)	70.926 (kmol/h)	95.228 (kmol/h)	95.228 (kmol/h)
Temperature setpoint	357.15 (K)	358.15 (K)	358.15 (K)	358.15 (K)
Pressure setpoint	6.428 (atm)	7.218 (atm)	8.886 (atm)	8.886 (atm)
Liquid level setpoint	2.119 (m)	1.998 (m)	2.426 (m)	2.426 (m)

Theorem validation through dynamic simulation

Numerical experiments were conducted to verify the steady-state agreement between MWD and the states as presented in the theorems. A dynamic simulation of the grade transition was carried out for the polymerization reactor shown in Figure 1. The process transitions from Grade A to Grade B under the operating conditions listed in Table 2. The input includes the feeds of catalyst, cocatalyst, monomer, hydrogen, and hexane, and three setpoints of PID controllers for reactor temperature, pressure, and liquid level. To simplify the operation, the step-change inputs of the dynamic simulation were set, that is, each input was changed sharply from the steady-state A value to the steady-state B value at the beginning of the transition. The simulation time was set to 50,000 s and the maximal chain length was set to 50,000. The computation was conducted using DASPK Solver on a DELL™ PowerEdge™ SC1425 system PC with a 2.8 GHz Intel® Xero™ CPU and 10 GB memory.

The dynamic simulation results of the key state variables, including the temperature, the concentrations of the monomer, the transfer agent, and the cocatalyst, the volume of reaction liquid, and the volume outflow rate, are shown in Figure 4. Results of another key state variable, the first moments of the living chain, are shown in Figure 5, where $Y1_1$, $Y1_2$, $Y1_3$, $Y1_4$, and $Y1_5$ represent the first moments of the living chains of the five active sites, and $Y1$ represents the summation of these first moments. The figures show that all of the variables vary from one steady state to another steady state. Because of the good performance of the temperature PID controller, the reactor temperature approaches the target temperature very quickly. The other state variables take relatively longer times to reach the new steady state. We can see the new steady state has been reached long before the end of the simulation time, 50,000 s.

The dynamic simulation results of the MWDs are also analyzed. Figure 6 illustrates how the dynamic MWD results change with time during grade transition from Grades A to B. In each subplot, the horizontal axis indicates the chain length in the logarithmic scale, $\log_{10}(\mathrm{mw} * n)$. Four MWD curves exist in each subplot, including the steady-state MWD at the beginning of the transition (i.e., the MWD of Grade A), the steady-state MWD at the end of the transition (i.e., the MWD of Grade B), the MWD at the current time obtained using the instantaneous Flory method, and the MWD at the current time obtained using the cumulative Flory method. The only exception is subplot 6(a), in which only two curves are presented as the current time is 0 s and the process is at state A. At 200 s, as illustrated in Figure 6b, the MWD curve of the instantaneous Flory method is distinct from the MWD curves of steady-state A and steady-state B because a step change occurs in the input variables. The instantaneous MWD curve represents only the newly generated polymer at this time point. The MWD result of the whole polymer in the reactor is represented by the dotted curve obtained by applying the cumulative Flory method on the dynamic MWD model. The cumulative MWD curve varies only slightly from that of the steady-state A; at 200 s, the total amount of the newly generated polymer barely influences the cumulative MWD, even though the instantaneous MWD has significantly changed. In Figure 6c, at time

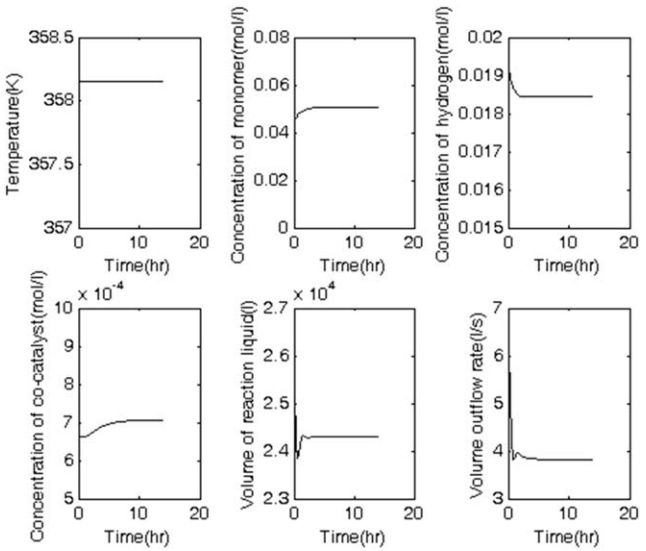

Figure 4. Dynamic simulation results of six state variables.

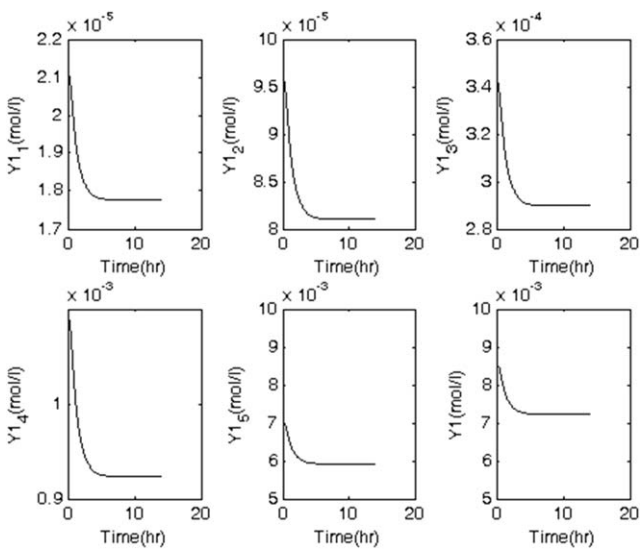

Figure 5. Dynamic simulation results of the first moments of the living chains.

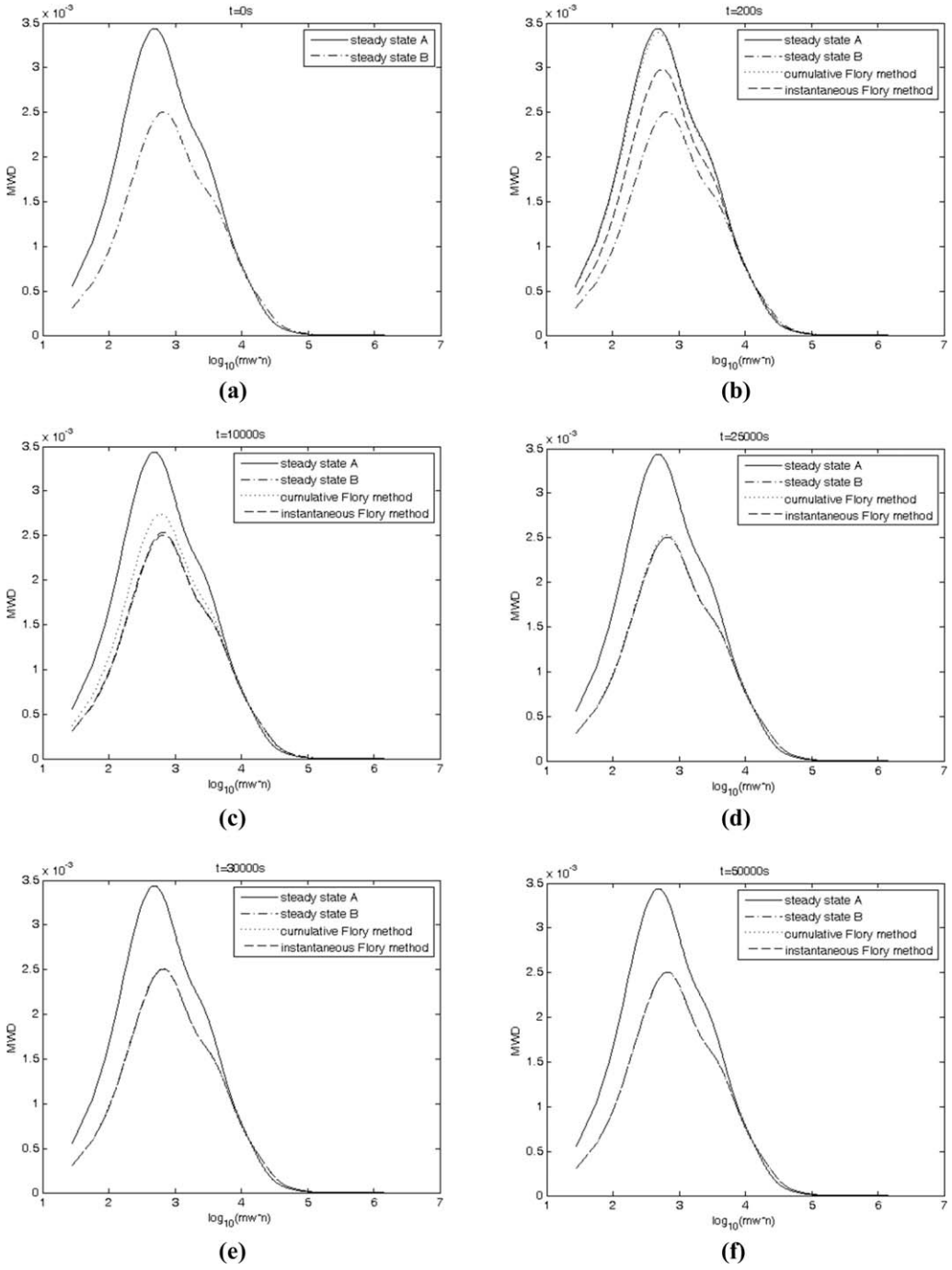

Figure 6. Dynamic MWD curves along time.

10,000 s, the instantaneous MWD is close to the target MWD but the cumulative MWD still shows a distinct difference. As the time increases to 25,000 s, (see Figure 6d), the instantaneous MWD overlaps with the target MWD, but the cumulative MWD still differs slightly from the target MWD. After 30,000 s, both the instantaneous and the cumulative MWD curves overlap with the target.

The dynamic simulation results show that the state variables and MWD results are fully synchronized. As shown in Theorem 2, bounded deviation from steady state on the state variables can guarantee bounded steady-state deviation on cumulative MWD. In Problem (87), η is used as the tolerance on the state variables to verify if a new steady state is reached. Following the previous numerical test, now consider the MWD deviation caused by η. We consider states at $t = 50{,}000$ s as the steady-state results and when the simulation time is close to 50,000 s, η can be specified very small. Moreover, we can relate η and δ in Problem (87) by comparing the results obtained at different time instants. As shown in Figure 7, δ varies monotonically with η and this result supports the conclusion derived in Theorem 2. Moreover, if we set η to 1% then from Figure 7 δ is about 0.85%, which is smaller than the error of the MWD measurement using GPC.

Dynamic Optimization on HDPE Slurry Process

The grade transition of the HDPE slurry process shown in Figure 1 is conducted using the proposed method. A

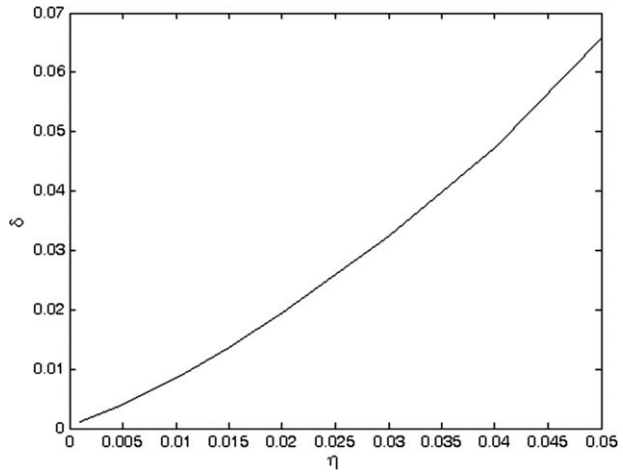

Figure 7. Relationship between η and δ.

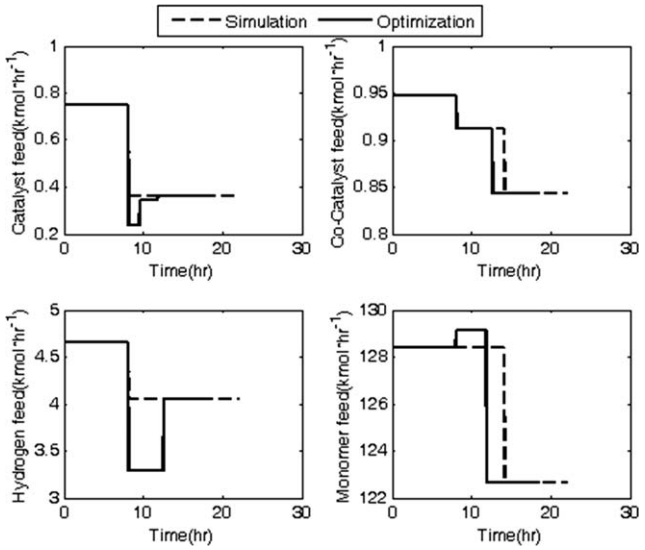

Figure 8. Comparison results of operating conditions of Grades C to D.

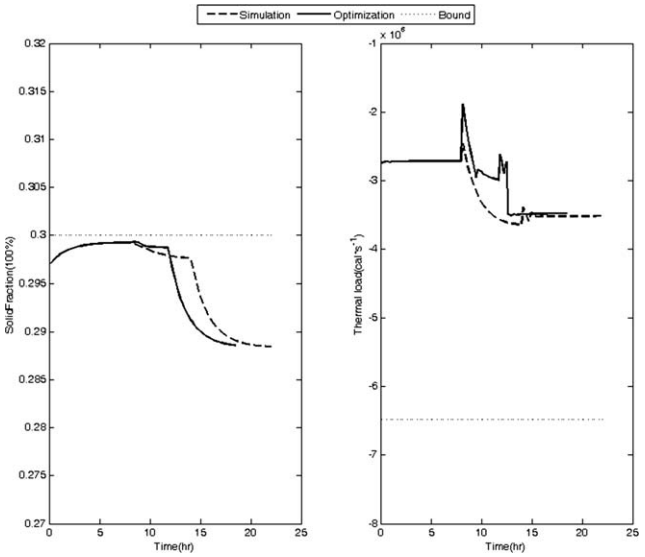

Figure 9. Constraints of the process conditions of Grades C to D.

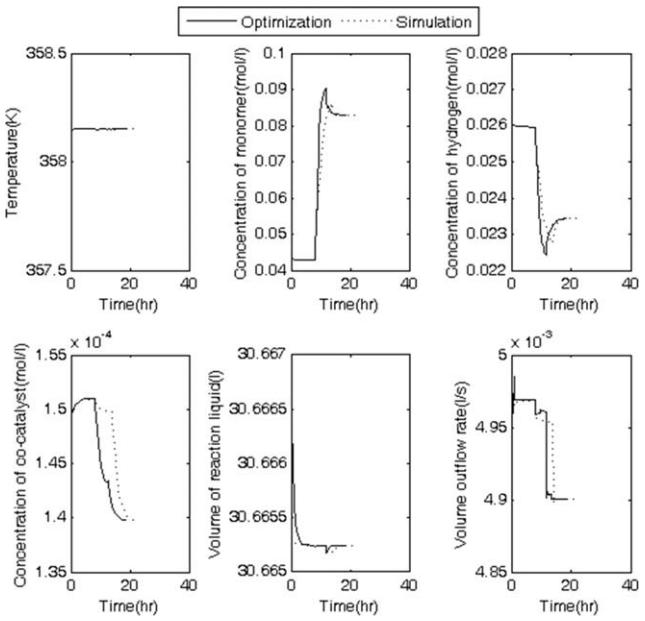

Figure 10. Dynamic results of six state variables of Grades C to D.

simultaneous discretization approach is used for dynamic optimization by transforming the differential-algebraic equations in (87) as a nonlinear programming (NLP) problem using orthogonal collocation on finite elements. The NLP model is coded and solved using AMPL (32-bit version) and Interior Point OPTimizer[39] version 3.8. The program is run on a Lenovo U410 PC with 64-bit Windows 7, 1.70 GHz Intel Core i5–3317U CPU, and 4.0 GB RAM.

Two grades from actual industrial data are used for the optimization of the grade transition. They are referred to as Grades C and D with the steady-state operating conditions also listed in Table 2. The manipulated variables include the feeds of catalyst, cocatalyst, hydrogen, and monomer. The

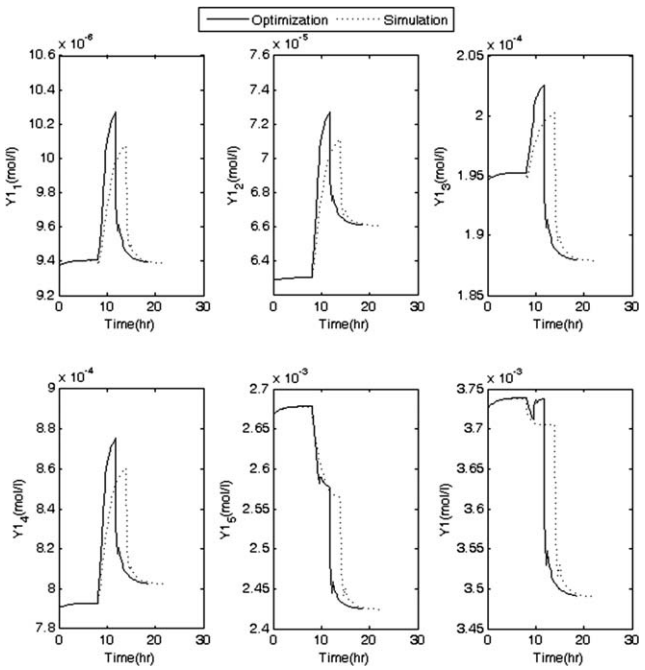

Figure 11. Dynamic results of the first moments of living chain of Grades C to D.

Table 3. Derivatives of $S(t_f)$

State Variable	Derivatives (C to D)	Derivatives (D to C)
Temperature	−2.112934e-10	4.282385e-11
Monomer	−6.575031e-09	3.946911e-11
Hydrogen	2.275823e-09	−7.454328e-10
Cocatalyst	−2.039525e-11	7.452239e-12
Volume	1.153329e-11	−2.055870e-12
Volume outflow	1.257037e-12	−1.109926e-13
$Y^1(1)$	−8.248387e-13	5.857114e-13
$Y^1(2)$	−6.359542e-12	4.704870e-12
$Y^1(3)$	−1.307295e-11	1.229704e-11
$Y^1(4)$	−6.865500e-11	5.501859e-11
$Y^1(5)$	−1.250536e-10	1.436252e-10
$Y^1(sum)$	−2.139659e-10	2.162314e-10

remaining inputs are set as constants shown in Table 2. The process is first set to the steady state of Grade C; then, grade transition begins after 8 h. Simulation of actual plant operations is also used as a comparison. The dynamic simulation results refer to those obtained using actual plant operational inputs, while the dynamic optimization results refer to the optimal results obtained using the proposed method.

Figure 8 compares the operating conditions of dynamic simulation and dynamic optimization of the transition from Grades C to D. In each subplot, the curves of simulation and optimization overlap for the first 8 h of operation before the transition. Thereafter, obvious differences can be observed. The results of both cases eventually overlap at the end of the transition, which agrees with the steady-state operating conditions of the target grade. Note that overshoot operations are required for the manipulated variables in the dynamic optimization to minimize the transition time.

In an actual industrial plant, some constraints in key state variables also exist for safety considerations. Figure 9 shows the results of solid fraction and thermal load with their required bounds. Here, solid fraction has an upper bound to ensure that the polymer is discharged from the reactor smoothly and the thermal load has a lower bound to ensure that polymerization is conducted normally and safely. Both constraints are satisfied by the dynamic simulation and optimization results, as shown in Figure 9.

The dynamic results of the key state variables in (87), including the temperature, the concentrations of monomer, transfer agent and cocatalyst, the liquid volume, and the outflow rate are shown in Figure 10. The information of the first

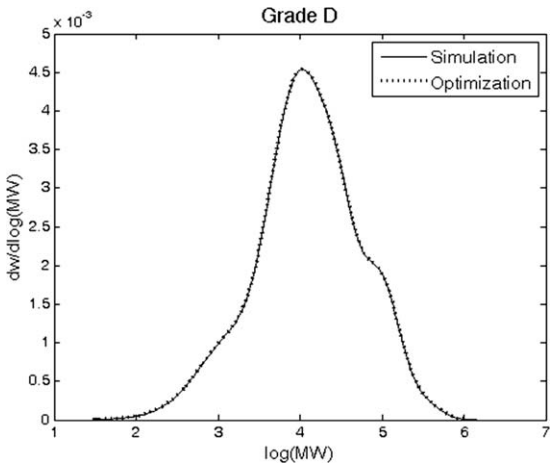

Figure 12. MWD results after transition to Grade D.

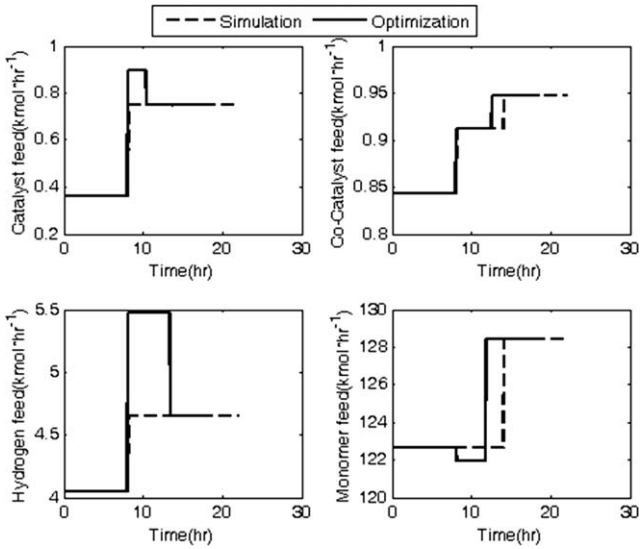

Figure 13. Comparison results of operating conditions of Grades D to C.

moment is illustrated in Figure 11. The figures show that all of the state variables vary from their initial steady state to their desired steady state. The derivatives of the aforementioned state variables at the final time are listed in Table 3. The derivatives of the state variables are essentially equal to zero. These results verify that the steady state was accomplished, which agrees with the first equality constraint in Problem (86).

After the dynamic optimization, the grade transition time between Grades C and D is shortened from 22 to 18.5 h. The reduction is almost 16% which is quite satisfactory. Further analysis shows that the results of Problem (87) with the instantaneous Flory distribution agree with the dynamic simulation results of the target grade as shown in Figure 12, even though the dynamic MWD model is not used in the proposed method. This further confirms that the proposed method can avoid arduous computational efforts when dealing with dynamic MWD optimization, while maintaining the precision of polymer quality.

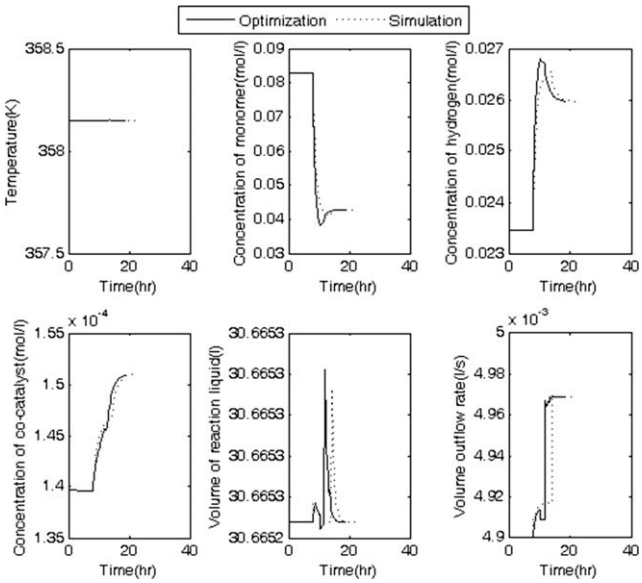

Figure 14. Dynamic results of six state variables of Grades D to C.

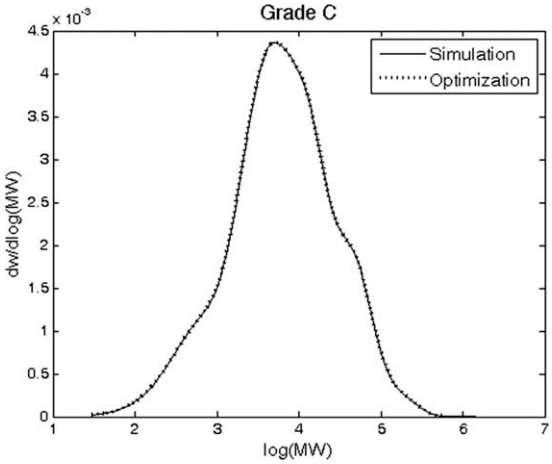

Figure 15. MWD results after transition to Grade C.

To further test the proposed method, grade transition from Grade D to Grade C is also conducted. First, dynamic simulation is conducted using the backward operation of Grades C to D. Then, dynamic optimization is conducted with the proposed method. The results of the manipulated variables are shown in Figure 13. Comparison with the results in Figure 8 reveals that the new optimization results are not the reverse operation of Grades C to D. Instead, overshoot operations in the opposite direction are used to save transition time. The dynamic results of six state variables are shown in Figure 14. We can see that both operations accomplish the transition. But compared with the reverse simulation operation, the optimized operation can obviously reduce the time. The MWD results are further compared in Figure 15, demonstrating the accuracy of the proposed method in dealing with MWD computation.

Conclusions

Accuracy and arduous computations of a dynamic optimization problem must be addressed when using dynamic optimization for grade transition processes based on MWDs. In this study, new theoretical results show the relationship between moment-based and dynamic MWD-based criteria. Moreover, a novel strategy featuring the moment method in cooperation with the instantaneous Flory distribution is proposed for dynamic optimization. This method guarantees grade transitions with detailed MWD information and avoids arduous computations for dynamic MWDs. Finally, the application of the proposed method on an HDPE slurry process is presented.

Acknowledgment

The authors gratefully acknowledge the financial support of 973 Program (No. 2012CB720500) and National Natural Science Foundation of China (Nos. 61374205 & 61074148).

Literature Cited

1. Takeda M, Ray WH. Optimal-grade transition strategies for multistage polyolefin reactors. *AIChE J*. 1999;45:1776–1793.
2. Asteasuain M, Brandolin A. High-pressure polymerization of ethylene in tubular reactors: a rigorous dynamic model able to predict the full molecular weight distribution. *Macromol React Eng*. 2009;3:398–411.
3. Kadam JV, Marquardt W, Srinivasan B, Bonvin D. Optimal grade transition in industrial polymerization processes via NCO tracking. *AIChE J*. 2007;53:627–639.
4. Cervantes C, Tonelli S, Brandonlin A, Bandoni JA, Biegler LT. Large-scale dynamic optimization for grade transition in a low density polyethylene plant. *Comput Chem Eng*. 2002;26:227–237.
5. Soares JBP, McKenna TFL. *Polyolefin Reaction Engineering*. Weinheim: Wiley-vch Verlag GmbH & Co. KGaA, 2012.
6. Ohshima M, Tanigaki M. Quality control of polymer production processes. *J Process Control*. 2000;10:135–148.
7. Chatzidoukas C, Perkins JD, Pistikopoulos EN, Kiparissides C. Optimal grade transition and selection of closed-loop controllers in a gas-phase olefin polymerization fluidized bed reactor. *Chem Eng Sci*. 2003;58:3643–3658.
8. Chatzidoukas C, Pistikopoulos S, Kiparssides C. A hierarchical optimization approach to optimal production scheduling in an industrial continuous olefin polymerization reactor. *Macromol React Eng*. 2009;3:36–46.
9. Lo DP, Ray WH. Dynamic modeling of polyethylene grade transition in fluidized bed reactors employing nickel-diimine catalysts. *Ind Eng Chem Res*. 2006;45:993–1008.
10. Ellis MF, Taylor TW, Jensen KF. On-line molecular weight distribution estimation and control in batch polymerization. *AIChE J*. 1994;40:445–462.
11. Crowley TJ, Choi KY. Calculation of molecular weight distribution from molecular weight moments in free radical polymerization. *Ind Eng Chem Res*. 1997;36:1419–1423.
12. Al-Harthi M, Soares JBP, Simon LC. Dynamic Monte Carlo simulation of ATRP with bifunctional initiators. *Macromol React Eng*. 2007;1:95–105.
13. Jianming L, Hongdong Z, Yuliang Y. Monte Carlo simulation of kinetics and chain-length distribution in radical polymerization. *Makromol Chem Theory Simul*. 1993;2:747–760.
14. Asteasuain M, Sarmoria C, Brandolin A. Recovery of molecular weight distributions from transformed domains. Part I. Application of pgf to mass balances describing reactions involving free radicals. *Polymer*. 2002;43:2513–2527.
15. Asteasuain M, Brandolin A, Sarmoria C. Recovery of molecular weight distributions from transformed domains. Part II. Application of numerical inversion methods. *Polymer*. 2002;43:2529–2541.
16. Miller NC, Toffolo RW, McAuley KB, McLellan PJ. Determining polymer chain length distributions using numerical inversion of Laplace transforms. *Polym React Eng*. 1996;4:279–301.
17. Mills PL. Determination of polymer chain length distributions by numerical inversion of z-transforms. *Comput Chem Eng*. 1986;10:399–420.
18. Deuflhard P, Wulkow M. Computational treatment of polyreaction kinetics by orthogonal polynomials of a discrete variable. *IMPACT Comput Sci Eng*. 1989;1:269–301.
19. Wulkow M. The simulation of molecular weight distributions in polyreaction kinetics by discrete Galerkin methods. *Macromol Theory Simul*. 1996;5:393–416.
20. Chen Z, Chen X, Shao Z, Yao Z, Biegler LT. Parallel calculation methods for molecular weight distribution of batch free radical polymerization. *Comput Chem Eng*. 2013;48:175–186.
21. Crowley TJ, Choi KY. Experimental studies on optimal molecular weight distribution control in a batch-free radical polymerization process. *Chem Eng Sci*. 1998;53:2769–2790.
22. Sayer C, Araujo PHH, Arzamendi G, Asua JM, Lima EL, Pinto JC. Modeling molecular weight distribution in emulsion polymerization reactions with transfer to polymer. *J Polym Sci Part A: Polym Chem*. 2001;39:3513–3528.
23. Vicente M, Sayer C, Leiza JR, Arzamendi G, Lima EL, Pinto JC, Asuaa JM. Dynamic optimization of non-linear emulsion copolymerization systems: open-loop control of composition and molecular weight distribution. *Chem Eng J*. 2002;85:339–349.
24. Kiparissides C, Seferlis P, Mourikas G, Morris AJ. Online optimizing control of molecular weight properties in batch free-radical polymerization reactors. *Ind Eng Chem Res*. 2002;20:6120–6131.
25. Soares JBP. Mathematical modeling of the microstructure of polyolefins made by coordination polymerization: a review. *Chem Eng Sci*. 2001;56:4131–4153.
26. Zapata-González I, Saldívar-Guerra E, Flores-Tlacuahuac A, Vivaldo-Lima E, Ortiz-Cisneros J. Efficient numerical integration of stiff differential equations in polymerization reaction engineering: computational aspects and applications. *Can J Chem Eng*. 2012;90:804–823.

27. Al-haj-Ali M, Ali E, Ajbar A, AlHumaizi K. Control of molecular weight distribution of polyethylene in gas-phase fluidized bed reactors. *Korean J Chem Eng*. 2010;27:364–372.
28. Pontes KV, Embiruçu M, Maciel R, Hartwich A, Marquardt W. Optimal process operation for the production of linear polyethylene resins with tailored molecular weight distribution. *AIChE J*. 2011;57:2149–2163.
29. Al-haj-Ali M, Ali E. Effect of monomer feed and production rate on the control of molecular weight distribution of polyethylene in gas phase reactors. *Comput Chem Eng*. 2011;35:2480–2490.
30. Touloupides V, Kanellopoulos V, Pladis P, Kiparissides C, Mignon D, Van-Grambezen P. Modeling and simulation of an industrial slurry-phase catalytic olefin polymerization reactor series. *Chem Eng Sci*. 2010;65:3208–3222.
31. Asteasuain M, Brandolin A. Modeling and optimization of a high-pressure ethylene polymerization reactor using gPROMS. *Comput Chem Eng*. 2008;32:396–408.
32. Khare NP, Seavey KC, Liu YA. Steady-state and dynamic modeling of commercial slurry high-density polyethylene (HDPE) processes. *Ind Eng Chem Res*. 2002;41:5601–5618.
33. Fontes CH, Mendes MJ. Analysis of an industrial continuous slurry reactor for ethylene-butene copolymerization. *Polymer*. 2005;46:2922–2932.
34. Zhang C, Zhan Z, Shao Z, Zhao Y, Chen X, Gu X, Yao Z, Feng L, Biegler LT. Equation-oriented optimization on an industrial high-density polyethylene slurry process with target molecular weight distribution. *Ind Eng Chem Res*. 2013;52:7240–7251.
35. Kim JH, Kim I, Woo SI. Computer simulation study of ethylene polymerization rate profile catalyzed over highly active Ziegler-Natta catalysts. *Ind Eng Chem Res*. 1991;30:2074–2079.
36. Hakim S, Moballegh L. Simulation of a series of industrial slurry reactors for HDPE polymerization process using deconvolution of the GPC graph of only the first reactor. *Iran Polym J*. 2006;15:655–666.
37. Flory PJ. *Principles of Polymer Chemistry*. New York: Cornell University Press, 1953.
38. Soares JBP, Hamielec AE. Deconvolution of chain-length distributions of linear polymers made by multiple-site-type catalysts. *Polymer*. 1995;36:2257–2263.
39. Biegler LT, Zavala VM. Large-scale nonlinear programming using IPOPT: an integrating framework for enterprise-wide dynamic optimization. *Comput Chem Eng*. 2009;33:575–582.

Manuscript received Sept. 23, 2013, and revision received Feb. 4, 2014.